Green Chemistry

PAPER

View Article Online
View Journal | View Issue

Cite this: *Green Chem.*, 2025, **27**, 15142

Sequential paired electrolysis-enabled synthesis of antifungal-active *gem*-difluoroalkenes *via* electrochemical halogen atom transfer

Fuyang Yue, Jiayi Li, Hongjian Song, Yuxiu Liu and Qingmin Wang *

Received 1st October 2025,
Accepted 20th October 2025

DOI: 10.1039/d5gc05189d

rsc.li/greenchem

Fluorine-containing compounds, particularly *gem*-difluoroalkenes—recognized as bioisosteres of carbonyl groups—hold crucial value in pharmaceuticals, agrochemicals, and functional materials, as they can modulate drug molecules' lipophilicity, pK_a, and bioavailability. Alkyl halides, indispensable building blocks in organic synthesis, serve as alkyl radical precursors; however, generating alkyl radicals from unactivated alkyl halides typically relies on costly photocatalysts, posing a notable challenge. This work presents a practical electrochemical method for the deiodinative *gem*-difluorovinylation of unactivated primary, secondary, and tertiary alkyl iodides. Operating under mild, transition-metal-free, and sacrificial-anode-free conditions, it integrates electrochemical halogen-atom transfer (e-XAT) with convergent paired electrolysis. The method exhibits broad substrate applicability and excellent compatibility with complex functional groups, enabling late-stage diversification of natural products, biomolecules, and pharmaceuticals. Additionally, glycoside-derived halides were used to synthesize *gem*-difluoroalkene derivatives; their antifungal activity was evaluated, with several active compounds identified, and preliminary mechanistic studies were conducted.

Green foundation

1. This work advances green chemistry *via* a mild, transition-metal/sacrificial-anode-free electrochemical method, using electricity as a traceless reagent, avoiding costly photocatalysts and toxic waste, and enabling late-stage diversification to cut synthetic steps.
2. As the electrochemical means is used, the use of oxidants and metal reagents is avoided. Paired electrolysis prevents the sacrifice of electrodes.
3. The adoption of renewable electricity, and the development of recyclable electrolytes reduce VOCs, carbon footprint, and waste could be investigated to further green the method.

Introduction

Fluorine-bearing compounds hold significant importance in the realms of pharmaceuticals, agrochemicals, and functional materials. They are capable of modulating the lipophilicity, pK_a, conformation, and bioavailability of drug molecules.[1] Specifically, *gem*-difluoroalkenes, often considered as bioisosteres of carbonyl groups, have attracted substantial attention during the drug discovery endeavor.[2] For instance, when the carbonyl group in artemisinin is replaced with a difluoroalkene group, the resulting compound exhibits antimalarial activity nearly double that of the original artemisinin[2] (as depicted in Fig. 1A). Additionally, the *gem*-difluoroalkene moiety serves as a valuable precursor. It can be readily converted into monofluoroalkene, difluoromethylene, difluorocyclopropane, and trifluoromethyl groups.[3] Given the wide-ranging applications of these compounds, there is an urgent need for effective synthetic methods to obtain highly functionalized *gem*-difluoroalkenes with diverse structures.

Alkyl halides are indispensable building blocks/reagents in organic synthesis and drug discovery, thanks to their structural diversity and easy synthetic access. Recently, they have served as alkyl radical precursors in radical-mediated transformations.[4] However, generating alkyl radicals from unactivated alkyl halides is challenging, mainly due to these halides' extremely low reduction potentials (E_{red} < −2.0 V *vs.* SCE). Current alkyl radical generation methods fall into two mechanistically distinct strategies: single-electron transfer (SET) and halogen-atom transfer (XAT). The SET approach is highly reliable in transition-metal catalysis[5] and photoredox systems[6] (Fig. 1B)—for example, MacMillan recently reported that metallaphotore-

State Key Laboratory of Elemento-Organic Chemistry, Research Institute of Elemento-Organic Chemistry, Frontiers Science Center for New Organic Matter, College of Chemistry, Nankai University, Tianjin 300071, People's Republic of China.
E-mail: wangqm@nankai.edu.cn

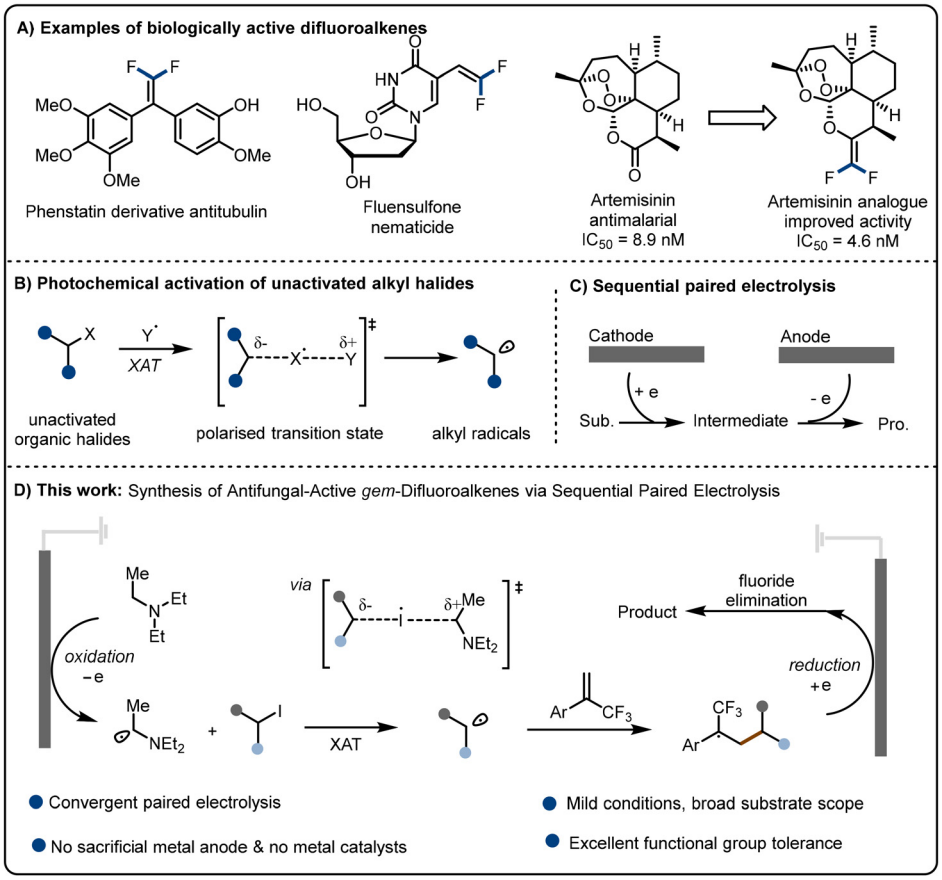

Fig. 1 From inspiration to reaction design. (A) Examples of biologically active difluoroalkenes. (B) Photochemical activation of unactivated alkyl halides. (C) Sequential paired electrolysis. (D) This work: synthesis of antifungal *gem*-difluoroalkenes *via* sequential paired electrolysis.

dox-activated transient silicon radicals facilitate alkyl radical generation from alkyl halides.[7] Most recently, Leonori and Juliá developed a method using nucleophilic α-aminoalkyl radicals (easily derived from simple amines in photoredox systems) as XAT agents, which drive homolytic C–halogen bond activation for alkyl radical formation under mild conditions.[8] However, all these strategies rely on costly photocatalysts (PC) to generate XAT agents. Thus, simpler, milder, and more efficient approaches to activate unactivated alkyl halides are still in high demand.

As a green and adjustable tool, electrosynthesis has attracted increasing interest. By employing electricity as a traceless redox reagent, it enables precise modulation of electron-transfer processes, offering robust backing for the discovery of novel chemical transformations.[9] In an undivided cell, a substrate can undergo sequential oxidation and reduction (or the reverse) at the corresponding electrode. Moreover, direct parallel paired electrolysis that involves a hydrogenation process to form the product (Fig. 1C) is commonly referred to as sequential paired electrolysis.[10]

Recently, progress has been made in the electrochemical halogen-atom transfer (e-XAT) strategy for the activation of unactivated alkyl iodides.[11] Building on this, we propose a convergent paired electrolysis system that integrates e-XAT with selective anodic and cathodic processes to achieve deiodinative *gem*-difluorovinylation of alkyl halides (Fig. 1D). During the submission of our manuscript, the Zheng group[12] reported a study that achieved the cross-coupling of alkyl radicals *via* the same halogen-atom transfer strategy and convergent paired electrolysis. Similar to their work, our method adopts a transition-metal-free electrochemical strategy, which eliminates the need for both sacrificial anodes and metal catalysts.

In this work, we report a sequential practical electrochemical method for the deiodinative *gem*-difluorovinylation of unactivated alkyl iodides (primary, secondary, and tertiary) *via* e-XAT and paired electrolysis under mild, transition-metal-free, and sacrificial-anode-free conditions. This method exhibits a broad substrate scope and excellent compatibility with complex functional groups, and has been further applied to the late-stage diversification of natural products, biomolecules, and pharmaceuticals. We selected glycoside-derived halides as starting materials to synthesize a series of *gem*-difluoroalkene derivatives. Given the novelty of their structures, we evaluated the antifungal activity of these compounds, identified several derivatives with promising activity, and conducted preliminary studies on their underlying mechanisms.

Results and discussion

The feasibility study of our hypothesis was performed by selecting 1-(benzyloxy)-4-(3,3,3-trifluoroprop-1-en-2-yl)benzene **1a** and (3*aS*,4*S*,6*R*,6*aR*)-4-(iodomethyl)-6-methoxy-2,2-dimethyltetrahydrofuro[3,4-*d*][1,3]dioxole **2a** as model substrates to investigate the reaction (Table 1). After systematic screening of the reaction parameters, we found that in an undivided cell with a carbon plate anode and a Pt plate cathode, defluorinative alkylation of **1a** for 8 h at a current of 3.0 mA occurred smoothly in an argon atmosphere at room temperature with tetrabutylammonium tetrafluoroborate as the electrolyte, Et_3N (Et_3N: E_{ox} = +0.77 V *vs.* SCE) as the XAT-agent precursor and CH_3CN as the solvent. Under these conditions, the desired product **3a** was generated in 79% isolated yield (entry 1). Control experiments verified the significance of electricity, the XAT-agent precursor, and the undivided cell for this transformation. Specifically, when electricity was absent (entry 2), the XAT-agent precursor was missing (entry 3), or a divided cell was used instead of an undivided one (entry 4), the reaction either did not occur or was severely affected. Replacing tetrabutylammonium tetrafluoroborate with other electrolytes as the supporting electrolyte under otherwise identical reaction conditions gave lower yields (entries 5–7). Adding a small amount of water to the reaction system did not increase the yield of the reaction (entry 8). Further optimizations were conducted by screening a variety of reaction solvents, such as DMSO, DCM, and HFIP, but they all provided unsatisfactory results (entries 9–11, respectively). Other electrode materials were found to be less effective (entries 12 and 13).

Table 1 Optimization of conditions for the reaction[a]

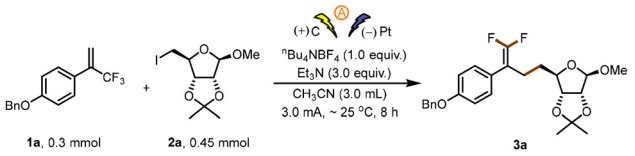

Entry	Deviation from standard conditions	Yield[b] (%)
1	None	81 (79[c])
2	No electricity	NR
3	No Et_3N	NR
4	Divided cell	NR
5	*n*-Bu_4NClO_4 as the electrolyte	72
6	*n*-Bu_4NPF_6 as the electrolyte	62
7	Me_4NBF_4 as the electrolyte	76
8	H_2O (0.2 mL) added	56
9	DMSO as the solvent	37
10	DCM as the solvent	51
11	HFIP as the solvent	11
12	RVC(+)–Zn(−)	30
13	RVC(+)–Pt(−)	80

[a] Reaction conditions, unless otherwise noted: in an undivided cell equipped with graphite plate electrodes, a solution of **1a** (0.3 mmol, 1 equiv.), **2a** (0.45 mmol, 1.5 equiv.), Et_3N (0.9 mmol, 3.0 equiv.) and *n*-Bu_4NBF_4 (0.3 mmol, 1.0 equiv.) in CH_3CN (3.0 mL) was electrolyzed at 3.0 mA with stirring for 8 h under argon at room temperature. [b] The yields were determined by ^{19}F NMR spectroscopy with fluorobenzene as an internal standard, NR = no reaction. [c] Isolated yield.

After confirmation of the optimized conditions, we turned our attention to the generality of the protocol (Fig. 2). Initially, α-trifluoromethyl arylalkenes bearing a wide range of functional groups were reacted with (3*aS*,4*S*,6*R*,6*aR*)-4-(iodomethyl)-6-methoxy-2,2-dimethyl-tetrahydrofuro[3,4-*d*][1,3] dioxole **2a** (Fig. 2). Electron-donating groups linked to the phenyl ring were tolerated well to give good yields of the corresponding *gem*-difluoroalkenes **3b–3h** (58–85%). However, when the *para*-substituents on the benzene ring were electron-withdrawing groups, the yields of the corresponding products (**3i** and **3j**) were slightly lower compared to those with electron-donating groups. When the *para*-substituents on the benzene ring were aryl groups, products **3k–3n** were obtained in moderate to good yields. The position of electron-donating substituents on the arylalkene has little effect on the yield; products **3o–3q** were obtained in 62–80% yields. Disubstituted arylalkenes gave **3r–3y** in moderate yields. Substrates containing functionalities useful for further synthetic manipulations, such as a dibenzothiophene (**3z**, 57%), a naphthalene ring (**3aa**, 79%) and a dimethylfluorene ring (**3ab**, 65%), were well tolerated. We further examined the generality of the proposed protocol by screening alkyl iodides and the results are summarized in Fig. 2. We tried many alkyl iodides with spirocyclic structures and some iodinated derivatives of drug molecules, and we found that products **3ac–3al** (58–80%) could be obtained in moderate to good yields. Meanwhile, this reaction was also well compatible with some simple alkyl iodides (**3am–3ao**, 69–85%). In addition, we employed our mild defluorinative alkylation approach to carry out functionalization on certain drug molecules, pesticides, and natural products with complex structures. As a result, the corresponding products (**3ap–3as**) were acquired in yields ranging from good to excellent. Overall, the outcomes presented in Fig. 2 illustrate the reliability of our method.

To clarify the practicality of these transformations, the gram scale synthesis of product **3a** was performed on a 4.0 mmol scale. The reaction proceeded smoothly to provide the desired product in 72% yield (Fig. 3a). Afterwards, control experiments were conducted to gain a more in-depth understanding of the reaction mechanism. When a radical scavenger such as TEMPO (2,2,6,6-tetramethylpiperidine-1-oxyl) or 1,1-diphenylethylene was introduced into the model reaction system, the reaction was significantly suppressed (Fig. 3b). Moreover, the captured products **4** and **5** were successfully detected using high-resolution mass spectrometry (HRMS).

Based on literature reports and our experimental observations, we propose the mechanism shown in Fig. 4. Initially, under standard electrochemical conditions, alkyl amine Et_3N undergoes anodic oxidation and deprotonation to generate α-amino alkyl radical **6**, which possesses strong nucleophilicity (E_{ox} = −1.12 V *vs.* SCE). Subsequently, α-amino alkyl radical **6** facilitates the formation of the corresponding alkyl radicals **7** *via* halogen-atom transfer with alkyl iodides. The exothermic dissociation of α-iodoamine into iminium iodide provides the

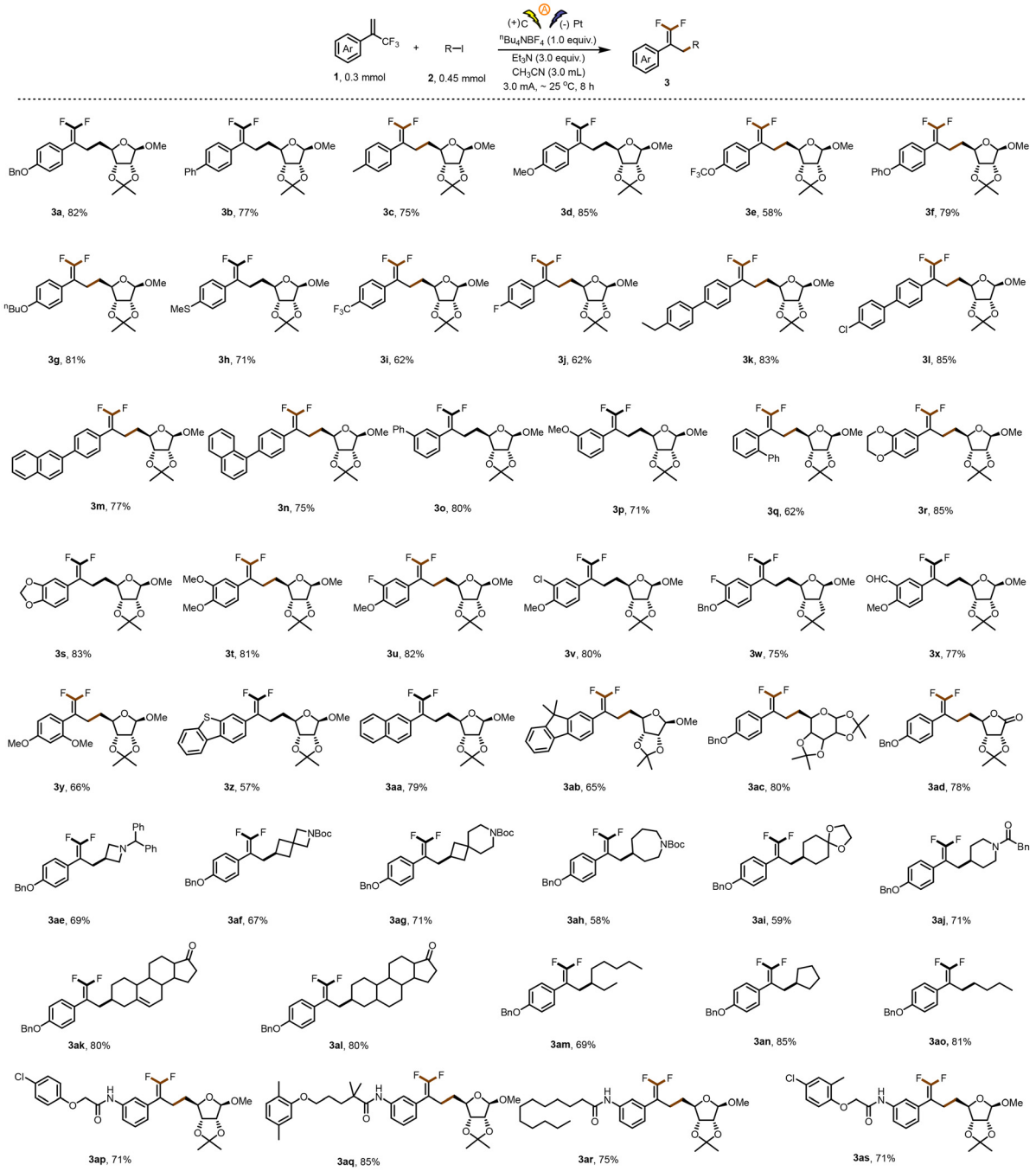

Fig. 2 Scope of the electrochemical halogen-atom transfer (e-XAT) alkylation. Reaction conditions, unless otherwise noted: carbon anode, Pt cathode, **1** (0.3 mmol), **2** (0.45 mmol), Et_3N (0.9 mmol, 3.0 equiv.), *n*-Bu_4NBF_4 (0.3 mmol, 1.0 equiv.), CH_3CN (3.0 mL), 3.0 mA, ~30 °C, 8 h. Isolated yields.

thermodynamic energy necessary to drive the process. Next, alkyl radical **7** adds to the α-trifluoromethyl alkene to produce CF_3-styrene carbon radical **8**. This radical is then reduced at the cathode to form CF_3-styrene carbanion intermediate **9**, which subsequently undergoes a β-fluoride elimination reaction to afford the target product.

The creation of new agrochemicals hinges on the discovery of novel drug skeletons with unique structures and mechanisms of action. Chitin is an essential component of fungal cell walls, and chitin synthase is crucial for regulating these walls and cell proliferation. This makes it an ideal target for fungicides. Polyoxins are a class of nucleoside antifungal agents produced by *Streptomycetes* which target chitin synthase. Their core structure consists of uracil and polyoxanone. To expand the structural diversity of fungal chitinase inhibitors, compounds containing difluoroalkyl glycosides

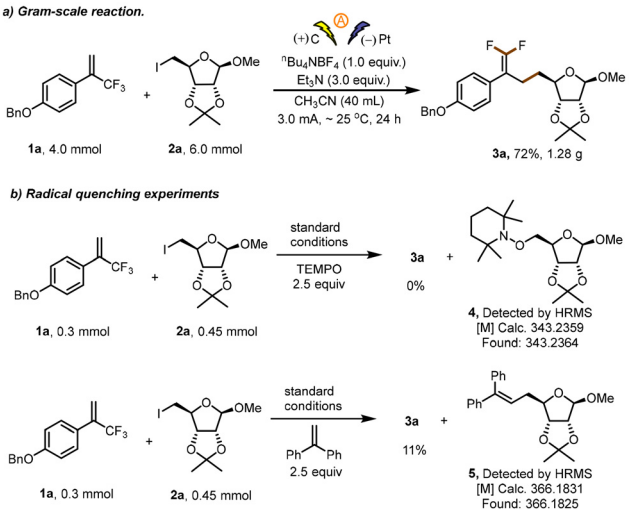

Fig. 3 (a) Gram-scale reaction and (b) radical quenching experiments.

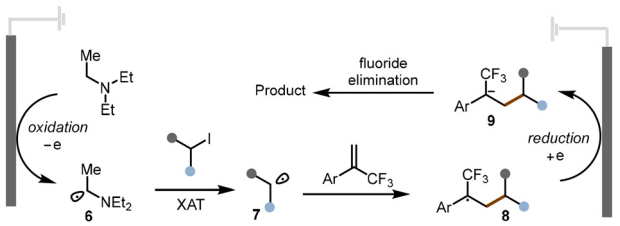

Fig. 4 Proposed mechanism.

were screened for antifungal activity and mechanism of action studies.

Target compounds were screened for bioactivity against eight important pathogenic fungi including *Alternaria solani*, *Botrytis cinerea*, *Cercospora arachidicola*, *Fusarium graminearum*, *Setosphaeria turcica*, *Pythium aphanidermatum*, *Rhizoctonia solani* and *Sclerotinia sclerotiorum* at a concentration of 50 μg mL^{-1} and the results are shown in Table S2. Polyoxin and pyraclostrobin were selected as positive controls. Polyoxin as well as compounds **3** showed moderate inhibitory effects against pathogenic fungi such as *C. arachidicola*, *F. graminearum*, *P. aphanidermatum*, *R. solani* and *S. sclerotiorum*. Compounds **3a**, **3b**, **3d**, **3j–3l**, **3n**, **3o**, **3t–3v**, **3aa–3ae**, and **3ai–3aj** showed more than 70.0% inhibition against *B. cinerea*, which was slightly higher than or comparable to that of polyoxin.

The inhibition rate of compound **3a** against *B. cinerea* was 98.2%, higher than the rate of the commercial fungicide pyraclostrobin (94.3%). Additionally, compounds **3b** and **3l** exhibited comparable inhibition rates of 73.1% and 72.5% against *S. turcica*, respectively, to those of polyoxin (72.5%). Furthermore, EC_{50} assays were conducted on the highly active compounds (Table 2). Compound **3b** exhibited moderate antifungal activity against *S. turcica*, with an EC_{50} value of 5.84 μg mL^{-1}, which is higher than those of polyoxin (2.25 μg mL^{-1}) and pyrazole (1.77 μg mL^{-1}). In contrast, compound **3a** displayed excellent antifungal activity against *B. cinerea*, with an EC_{50} value of 2.01 μg mL^{-1}—superior to that of polyoxin (3.02 μg mL^{-1}), but slightly less potent than pyraclostrobin (1.30 μg mL^{-1}). Therefore, compound **3a** was selected for mechanism of action studies.

The chitin synthase protein of *B. cinerea* was modelled using AlphaFold2. Molecular docking was then performed using AutoDock and the results were visualised. The molecular docking results showed that both compound **3a** and polyoxins bind to the active pocket of chitin synthase, with respective binding energies of −9.6 and −10.8 kcal mol^{-1}. As demonstrated in Fig. 5A and B, compound **3a** and polyoxins both form hydrogen bond interactions with ARG1027. Molecular dynamics simulations were performed using GROMACS software to investigate the conformational stability and dynamic behaviour of the ligand–*B. cinerea* chitinase complex. The RMSD values were calculated using the 50 ns molecular dynamics simulation. Fig. 5C shows that the protein RMSD in the compound **3a** complex increases rapidly within the first 5 ns and then stabilises at around 1.0 Å, whereas the protein

Table 2 *In vitro* EC_{50} values of selected compounds

Fungi	Compd	Regression equation	*R*	95% confidence interval (μg mL^{-1})	EC_{50} (μg mL^{-1})
Botrytis cinerea	**3a**	$y = 4.790 + 0.691x$	0.9963	1.65–2.46	2.01
	3b	$y = 4.134 + 0.947x$	0.9916	7.02–9.61	8.21
	3d	$y = 4.077 + 1.163x$	0.9927	5.37–7.21	6.22
	3f	$y = 4.064 + 1.191x$	0.9815	4.82–7.75	6.11
	3d	$y = 4.077 + 1.163x$	0.9927	5.37–7.21	6.22
	3k	$y = 3.137 + 1.336x$	0.9784	17.91–34.32	24.79
	3o	$y = 3.597 + 1.1574x$	0.9862	12.71–20.89	16.29
	3t	$y = 4.076 + 0.855x$	0.9915	10.09–14.37	12.04
	3u	$y = 3.960 + 1.183x$	0.9883	6.27–9.15	7.57
	3v	$y = 3.885 + 1.247x$	0.9639	5.58–11.01	7.84
	3ae	$y = 4.351 + 1.286x$	0.9958	2.83–3.62	3.20
	3aj	$y = 3.501 + 1.262x$	0.9941	13.39–17.69	15.39
	Polyoxin	$y = 3.784 + 2.417x$	0.9592	2.14–4.74	3.18
Exserohilum turcicum	**3b**	$y = 4.186 + 1.063x$	0.9827	4.64–7.34	5.84
	3l	$y = 3.510 + 1.308x$	0.9752	10.70–17.74	13.77
	Polyoxin	$y = 4.481 + 1.474x$	0.9886	1.91–2.65	2.25

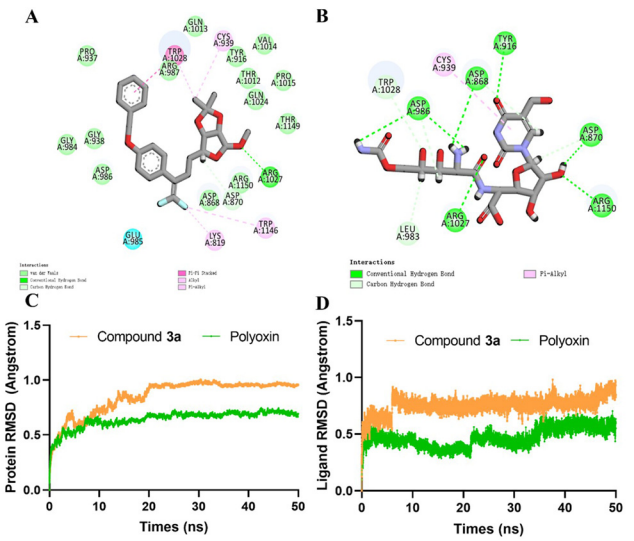

Fig. 5 Binding modes of target compounds to *B. cinerea* chitin synthetase. Binding modes of compound **3a** (A) and polyoxins (B) to *B. cinerea* chitin synthetase. RSMD plots (C and D) of the protein–ligand complex during 50 ns MD simulation.

RMSD in the polyoxin complex remains consistently at around 0.6 Å with minimal fluctuations. This indicates that the polyoxin complex exhibits superior conformational stability. Fig. 5D shows that the ligand RMSD of compound **3a** fluctuates between 0.6 and 1.0 Å, indicating high conformational flexibility and less stable binding than polyoxins. While compound **3a** forms a relatively stable protein–ligand complex, significant conformational fluctuations during binding may impact its binding affinity and biological activity.

Subsequently, scanning electron microscopy (SEM) and transmission electron microscopy (TEM) were employed to examine the morphological and ultrastructural alterations in the *B. cinerea* mycelium following treatment with compound **3a**. SEM images (Fig. 6A and B) revealed that the hyphae in the control group exhibited a smooth surface and intact morphology. By contrast, significant surface damage was evident in the hyphae treated with compound **3a**, including shrinkage, wrinkling, and collapse of the hyphal structure. This indicated that the integrity of the cell wall had been compromised. TEM results showed that the control cells exhibited well-defined intracellular structures, including intact cell walls (CW), clear cytoplasmic boundaries, and uniformly distributed organelles (Fig. 6C). In contrast, fungal cells treated with compound **3a** displayed thinned cell walls, plasmolysis, cytoplasmic vacuolisation, and organelle disintegration (Fig. 6D). These structural changes suggested that compound **3a** disrupted the integrity of the fungal cell wall. Docking results showed that compound **3a** interacted with the active site of chitin synthase. These findings indicate that its antifungal activity may be mediated by chitin synthase inhibition, thereby impairing chitin biosynthesis and compromising the cell wall.

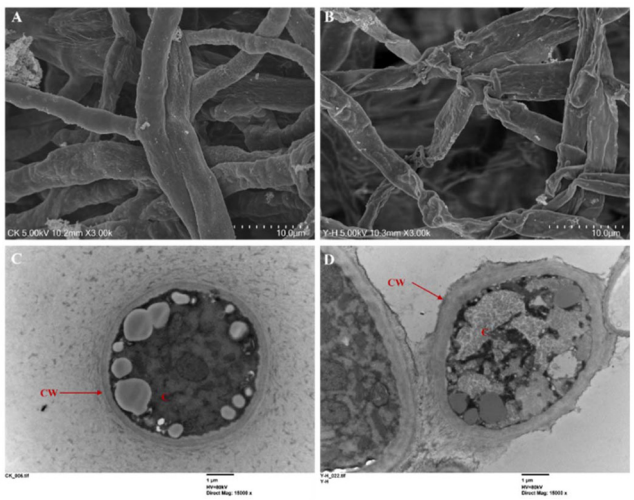

Fig. 6 Scanning electron micrographs and transmission electron micrographs of *B. cinerea* mycelia: (A) scanning electron micrograph of *B. cinerea*: control, 0.5% DMF, 3000×; (B) scanning electron micrograph of *B. cinerea*: treated with 0.5% DMF plus compound **3a** at 2.01 μg mL^{-1}, 3000×; (C) transmission electron micrograph of *B. cinerea*: control, 0.5% DMF, 15 000×; and (D) transmission electron micrograph of *B. cinerea*: treated with 0.5% DMF plus compound **3a** at 2.01 μg mL^{-1}, 15 000×. CW: cell wall; C: cytoplasm.

Conclusions

This study developed a green electrochemical method for deiodinative *gem*-difluorovinylation of unactivated alkyl iodides *via* e-XAT and convergent paired electrolysis, under mild, transition-metal-free, sacrificial-anode-free conditions, solving the problem of activating such alkyl halides without costly photocatalysts. It has a broad substrate scope, enabling late-stage diversification of natural products and drugs, with gram-scale synthesis feasible. Glycoside-derived *gem*-difluoroalkene derivatives showed good antifungal activity, *e.g.*, **3a** against *B. cinerea* (EC_{50} = 2.01 μg mL^{-1}) outperforming polyoxin. Mechanistic studies confirmed radical pathways and that **3a** inhibited chitin synthase. This work aids *gem*-difluoroalkene synthesis and new antifungal development.

Author contributions

F. Y. conceived the chemistry and designed the experiments under the guidance of Professor Q. W. The experiments and data analysis were conducted by all authors. F. Y. wrote the manuscript. All authors gave approval to the final version of the manuscript.

Conflicts of interest

There are no conflicts to declare.

Date availability

All relevant data are presented in the article and its supplementary information (SI). Supplementary information: general comments, general procedures, optimization details and NMR spectra. See DOI: https://doi.org/10.1039/d5gc05189d.

Acknowledgements

We are grateful to the National Natural Science Foundation of China (22271166) and Tianjin Science and Technology Plan Project Technology Innovation Guidance Special Fund (25YDTPJC00600) for generous financial support for our programs.

References

1 (*a*) Y. Pan, J. Qiu and R. B. Silverman, *J. Med. Chem.*, 2003, **46**, 5292; (*b*) P. Jeschke, *ChemBioChem*, 2004, **5**, 570; (*c*) Y. Ogawa, E. Tokunaga, O. Kobayashi, K. Hirai and N. Shibata, *iScience*, 2020, **23**, 101467; (*d*) Q. Wang, H. Song and Q. Wang, *Chin. Chem. Lett.*, 2022, **33**, 626–642; (*e*) S. Purser, R. Moore, S. Swallow and V. Gouverneur, *Chem. Soc. Rev.*, 2008, **37**, 320.

2 (*a*) W. R. Moore, G. L. Schatzman, E. T. Jarvi, R. S. Gross and J. R. McCarthy, *J. Am. Chem. Soc.*, 1992, **114**, 360; (*b*) P. Jeschke, *Pest Manage. Sci.*, 2010, **66**, 10; (*c*) F. Yue, H. Ma, P. Ding, H. Song, Y. Liu and Q. Wang, *ACS Cent. Sci.*, 2023, **9**, 2268–2276.

3 (*a*) J. Wu, S. Zhang, H. Gao, Z. Qi, C. Zhou, W. Ji, Y. Liu, Y. Chen, Q. Li, X. Li and H. Wang, *J. Am. Chem. Soc.*, 2017, **139**, 3537; (*b*) J. Liu, J. Yang, F. Ferretti, R. Jackstell and M. Beller, *Angew. Chem., Int. Ed.*, 2019, **58**, 4690; (*c*) T. Fujita, K. Fuchibe and J. Ichikawa, *Angew. Chem., Int. Ed.*, 2019, **58**, 390; (*d*) F. Tian, G. Yan and J. Yu, *Chem. Commun.*, 2019, **55**, 13486; (*e*) F. Yue, J. Liu, H. Ma, Y. Liu, J. Dong and Q. Wang, *Org. Lett.*, 2022, **24**, 4019–4023; (*f*) W. Tang and P. Fan, *Org. Lett.*, 2023, **25**, 5756; (*g*) F. Yue, M. Li, K. Yang, H. Song, Y. Liu and Q. Wang, *Chem. Sci.*, 2024, **15**, 14241–14247.

4 (*a*) G. C. Fu, *ACS Cent. Sci.*, 2017, **3**, 692–700; (*b*) D. J. Weix, *Acc. Chem. Res.*, 2015, **48**, 1767–1775; (*c*) M. R. Kwiatkowski and E. J. Alexanian, *Acc. Chem. Res.*, 2019, **52**, 1134–1144; (*d*) P. Chuentragool, D. Kurandina and V. Gevorgyan, *Angew. Chem., Int. Ed.*, 2019, **58**, 11586–11598; (*e*) F. Yue, M. Li, F. Yuan, H. Song, Y. Liu and Q. Wang, *Chin. Chem. Lett.*, 2025, **36**, 111053.

5 (*a*) H. Chen, X. Jia, Y. Yu, Q. Qian and H. Gong, *Angew. Chem., Int. Ed.*, 2017, **56**, 13103–13106; (*b*) F. Zhou, J. Zhu, Y. Zhang and S. Zhu, *Angew. Chem., Int. Ed.*, 2018, **57**, 4058–4062; (*c*) S. Bera, R. Mao and X. Hu, *Nat. Chem.*, 2021, **13**, 270–277; (*d*) D. Qian, S. Bera and X. Hu, *J. Am. Chem. Soc.*, 2021, **143**, 1959–1967; (*e*) X. Wu, W. Hao, K. Ye, B. Jiang, G. Pombar, Z. Song and S. Lin, *J. Am. Chem. Soc.*, 2018, **140**, 14836–14843; (*f*) A. Cai, W. Yan, C. Wang and W. Liu, *Angew. Chem., Int. Ed.*, 2021, **60**, 27070–27077.

6 (*a*) J. D. Nguyen, E. M. D'Amato, J. M. R. Narayanam and C. R. J. Stephenson, *Nat. Chem.*, 2012, **4**, 854–859; (*b*) H. Kim and C. Lee, *Angew. Chem., Int. Ed.*, 2012, **51**, 12303–12306.

7 (*a*) P. Zhang, C. C. Le and D. W. C. MacMillan, *J. Am. Chem. Soc.*, 2016, **138**, 8084–8087; (*b*) D. J. P. Kornfilt and D. W. C. MacMillan, *J. Am. Chem. Soc.*, 2019, **141**, 6853–6858; (*c*) G. H. Lovett, S. Chen, X.-S. Xue, K. N. Houk and D. W. C. MacMillan, *J. Am. Chem. Soc.*, 2019, **141**, 20031–20036; (*d*) H. A. Sakai, W. Liu, C. C. Le and D. W. C. MacMillan, *J. Am. Chem. Soc.*, 2020, **142**, 11691–11697.

8 (*a*) B. Górski, A.-L. Barthelemy, J. J. Douglas, F. Juliá and D. Leonori, *Nat. Catal.*, 2021, **4**, 623–630; (*b*) Z. Zhang, B. Górski and D. Leonori, *J. Am. Chem. Soc.*, 2022, **144**, 1986–1992.

9 (*a*) R. Francke and R. D. Little, *Chem. Soc. Rev.*, 2014, **43**, 2492–2521; (*b*) R. Feng, J. A. Smith and K. D. Moeller, *Acc. Chem. Res.*, 2017, **50**, 2346–2352; (*c*) M. Yan, Y. Kawamata and P. S. Baran, *Chem. Rev.*, 2017, **117**, 13230–13319; (*d*) J. C. Siu, N. Fu and S. Lin, *Acc. Chem. Res.*, 2020, **53**, 547–560; (*e*) H. Wang, X. Gao, Z. Lv, T. Abdelilah and A. Lei, *Chem. Rev.*, 2019, **119**, 6769–6787; (*f*) P. Xiong and H.-C. Xu, *Acc. Chem. Res.*, 2019, **52**, 3339–3350; (*g*) L. Ackermann, *Acc. Chem. Res.*, 2020, **53**, 84–104; (*h*) K.-J. Jiao, Y.-K. Xing, Q.-L. Yang, H. Qiu and T. Mei, *Acc. Chem. Res.*, 2020, **53**, 300–310; (*i*) X.-Q. Zhou, H.-T. Tang, F.-H. Cui, Y. Liang, S.-H. Li and Y.-M. Pan, *Green Chem.*, 2023, **25**, 5024–5029; (*j*) W.-J. Wei, X.-Y. Wang, H.-T. Tang, F.-H. Cui, Y.-Q. Wu and Y.-M. Pan, *Sci. China: Chem.*, 2024, **67**, 3382–3388.

10 (*a*) B. Wang, X. Zhang, Y. Cao, L. Zou, X. Qi and Q. Lu, *Angew. Chem., Int. Ed.*, 2023, **62**, e202218179; (*b*) Z. Liu, X. Zhu, J. Guo, C. Ma, Z. Zuo and T. Mei, *Sci. Bull.*, 2024, **69**, 1866–1874; (*c*) D. Wood and S. Lin, *Angew. Chem., Int. Ed.*, 2023, **62**, e202218858; (*d*) R. Zhang, L. Li, K. Zhou and N. Fu, *Chem. – Eur. J.*, 2023, **29**, e202301034.

11 X. Sun and K. Zheng, *Nat. Commun.*, 2023, **14**, 6825.

12 X. Sun and K. Zheng, *J. Am. Chem. Soc.*, 2025, **147**, 34767–34776.

